Article

Properties of Inhibitors of Methane Hydrate Formation via Molecular Dynamics Simulations

Brian J. Anderson, Jefferson W. Tester, Gian Paolo Borghi, and Bernhardt L. Trout

J. Am. Chem. Soc., **2005**, 127 (50), 17852-17862• DOI: 10.1021/ja0554965 • Publication Date (Web): 19 November 2005

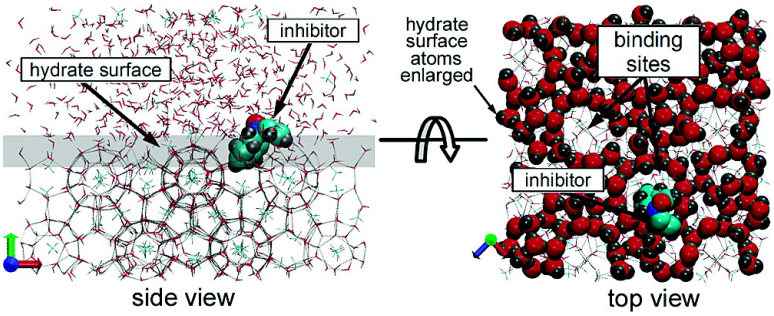

More About This Article

Additional resources and features associated with this article are available within the HTML version:

- Supporting Information
- Links to the 7 articles that cite this article, as of the time of this article download
- Access to high resolution figures
- Links to articles and content related to this article
- Copyright permission to reproduce figures and/or text from this article

View the Full Text HTML

J|A|C|S
ARTICLES
Published on Web 11/19/2005

Properties of Inhibitors of Methane Hydrate Formation via Molecular Dynamics Simulations

Brian J. Anderson,[†] Jefferson W. Tester,[†] Gian Paolo Borghi,[‡] and Bernhardt L. Trout*[,†]

Contribution from the Department of Chemical Engineering, Massachusetts Institute of Technology, 77 Massachusetts Avenue 66-458, Cambridge, Massachusetts 02139, and Center for Upstream Oil & Gas Technologies, EniTecnologie S.p.A., via Maritano 26 20097, San Donato Milanese (MI), Italy

Received August 11, 2005; E-mail: trout@mit.edu.

Abstract: Within the framework of a proposed two-step mechanism for hydrate inhibition, the energy of binding of four inhibitor molecules (PEO, PVP, PVCap, and VIMA) to a hydrate surface is estimated with molecular dynamic simulations. One key feature of this proposed mechanism is that the binding of an inhibitor molecule to the surface of an ensuing hydrate crystal disrupts growth and therein crystallization. It is found through the molecular dynamic simulations that inhibitor molecules that experimentally exhibit better inhibition strength also have higher free energies of binding, an indirect confirmation of our proposed mechanism. Inhibitors increasing in effectiveness, PEO < PVP < PVCap < VIMA, have increasingly negative (exothermic) binding energies of $-0.2 < -20.6 < -37.5 < -45.8$ kcal/mol and binding free energies of increasing favorability ($+0.4 \approx +0.5 < -9.4 < -15.1$ kcal/mol). Furthermore, the effect of an inhibitor molecule on the local liquid water structure under hydrate-forming conditions was examined and correlated to the experimental effectiveness of the inhibitors. Two molecular characteristics that lead to strongly binding inhibitors were found: (1) a charge distribution on the edge of the inhibitor that mimics the charge separation in the water molecules on the surface of the hydrate and (2) the congruence of the size of the inhibitor with respect to the available space at the hydrate-surface binding site. Equipped with this molecular-level understanding of the process of hydrate inhibition via low-dosage kinetic hydrate inhibitors we can design new, more effective inhibitor molecules.

Introduction

Natural gas water clathrates or gas hydrates are systems of polyhedral cells formed by hydrogen-bonded water molecules and stabilized by encaged guest molecules, such as methane and/or carbon dioxide (Figures 1 and 2). They are of tremendous relevance in diverse areas such as energy, the environment, astrophysics, geology, and marine ecosystems.[1−4] The existence of clathrate hydrates was first documented by Sir Humphrey Davy[5] in 1811, who observed that a solution of chlorine gas in water freezes more readily than pure water. Since 1939, when Hammerschmidt[6] concluded that natural gas hydrates were blocking gas transmission lines, the susceptibility of forming solid hydrates in gas transmission lines under normal operating conditions has led to many investigations aimed at understanding and avoiding hydrate formation, an area of ongoing research. The optimization of natural gas production and transmission operations depends on the ability to make quantitative predictions of the rates of formation of solid hydrates as a function of temperature, pressure, and composition, including the effects of additives designed to inhibit the formation of hydrates.

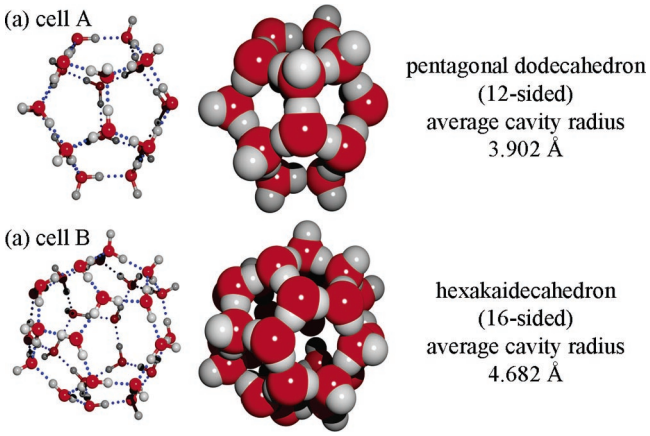

Figure 1. Cavities of structure II clathrates. This study focuses on the structure II hydrate because that is the form formed by natural gas that is typically a mixture of roughly 95% CH_4, 2.5% C_2H_6, 1.5% N_2, and the balance C_3H_8 and trace gases.

Annually, oil and gas companies spend over 500 million U.S. dollars on hydrate prevention via methanol injection. Typically, large amounts (up to 50 vol %) of methanol are used to help avoid hydrate plugging by lowering the formation temperature, with significant economic costs and potential environmental

[†] Massachusetts Institute of Technology.
[‡] EniTecnologie S.p.A.

(1) Sloan, E. D., Jr. *Clathrate Hydrates of Natural Gases*, 2nd ed.; Marcel Dekker: New York, 1998.
(2) Buffett, B. A. *Annu. Rev. Earth Planet. Sci.* **2000**, *28*, 477−507.
(3) Kvenvolden, K. A. *Rev. Geophys.* **1993**, *31*, 173−187.
(4) Miller, S. L. *Science* **1970**, *170*, 531.
(5) Davy, H. *Philos. Trans. R. Soc. London* **1811**, *101*, 1−35.
(6) Hammerschmidt, E. G. *Ind. Eng. Chem.* **1934**, *26*, 851−855.

10.1021/ja0554965 CCC: $30.25

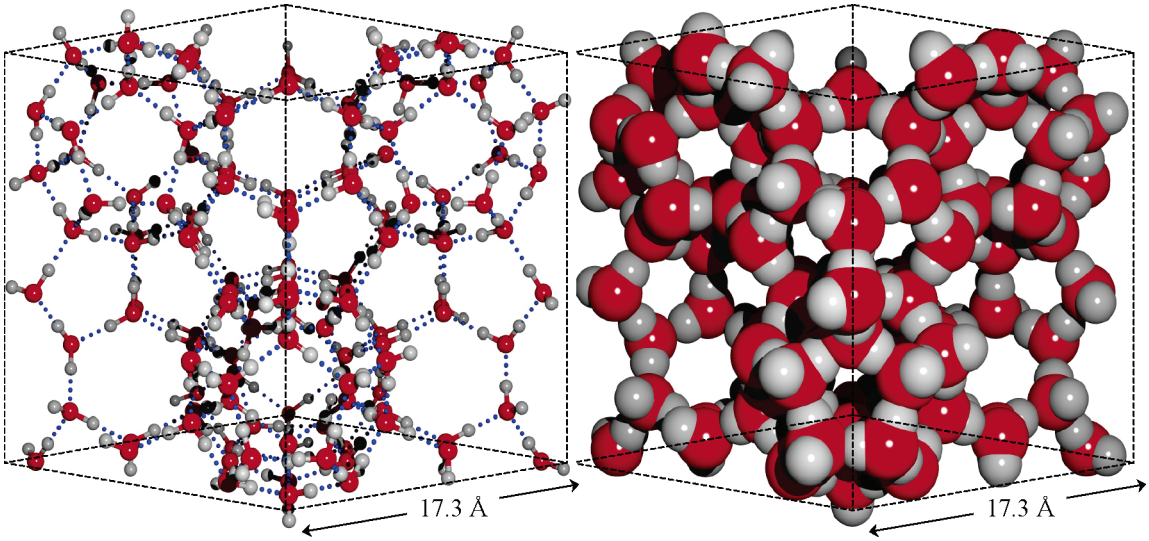

Figure 2. Ball-and-stick and space-filling models of a unit cell of the structure II clathrate with a lattice constant of 17.3 Å. Consists of 136 water molecules that form 16 pentagonal dodecahedral cavities (cell A) and 8 hexakaidecahedral cavities (cell B); thus, for a completely occupied system, the ideal stoichiometry would be (16A,8B)·136 H_2O.

effects. The lowering of the hydrate-formation temperature in the presence of methanol reflects the thermodynamic effect of methanol on reducing the chemical potential of water in the liquid-phase mixture, resulting in a freezing point depression of the solid hydrate phase.

In the last 15 years or so, many research efforts have been focused on developing what are termed "low-dosage hydrate inhibitors", or LDHIs, that can kinetically inhibit hydrate formation.[7] LDHIs operate much differently than thermodynamic inhibitors such as methanol. They are often effective at concentrations as low as 0.5 wt %[7] and act by delaying the onset of hydrate formation, whereas thermodynamic inhibitors are effective only at much higher concentrations and act by changing the conditions of hydrate thermodynamic stability.

Understanding the nucleation and growth of hydrates is a challenge that is just starting to be met and has tremendous scientific and technological ramifications. Noting that current experimental technology is not able to capture the nucleation process of clathrate−hydrates, we developed a molecular simulation approach based on sophisticated methods from theoretical chemistry to do so.[8−10] Recently, Rodger's group at Warwick[11,12] used molecular simulations and found that LDHIs (specifically tributylammoniumpropylsulfonate [TBAPS], polyvinyl pyrollidone [PVP], polyvinyl caprolactam [PVCap], and poly(dimethylaminoethyl methacrylate) [PDMAEMA]) reduce the degree of structure in the surrounding water which would presumably increase the barrier to hydrate nucleation. This study focuses on the action of LDHIs on ensuing crystallites of hydrates within a reasonable framework of nucleation and crystallization.

Proposed Inhibition Mechanism

There have been much discussion and disagreement regarding the mechanism by which LDHIs inhibit hydrate formation.[11,13−17] Furthermore, no proposed mechanism fully explains all of the phenomena associated with hydrate kinetic inhibition such as increased induction time with sudden growth coupled with the crystal morphology changes observed in inhibited growth conditions.[11,18−20] The following section outlines a proposed mechanism that will act as a framework for our study of the factors that control hydrate-inhibition properties.

The formation of natural gas hydrates begins with either a heterogeneous or homogeneous nucleation event. Previous work in our group at MIT[8] concluded that nucleation proceeds via ''the local structuring mechanism", i.e. a thermal fluctuation causing the local ordering of guest molecules leads to the nucleation of the clathrate, and not by the previous conceptual picture, called ''the labile cluster hypothesis" proposed by Sloan and others.[1,21−23] Our statistical approach is also contrasted with classical nucleation theory, in which macroscopic properties are assumed to describe systems of dimensions on the order of angstroms.

Similar to the classical theory of nucleation, our approach treats nucleation as an activated event, which is more or less irreversible. Once the system surpasses the free energy barrier to nucleation, crystal growth occurs. Within that context, the

(7) Lederhos, J. P.; Long, J. P.; Sum, A.; Christiansen, R. L.; Sloan, E. D. *Chem. Eng. Sci.* **1996**, *51*, 1221−1229.
(8) Radhakrishnan, R.; Trout, B. L. *J. Chem. Phys.* **2002**, *117*, 1786−1796.
(9) Radhakrishnan, R.; Trout, B. L. *Phys. Rev. Lett.* **2003**, *90*, 158301/1−158301/4.
(10) Radhakrishnan, R.; Trout, B. L. *J. Am. Chem. Soc.* **2003**, *125*, 7743−7747.
(11) Storr, M. T.; Taylor, P. C.; Monfort, J. P.; Rodger, P. M. *Journal of the American Chemical Society* **2004**, *126*, 1569−1576.
(12) Hawtin, R. W.; Moon, C.; Rodger, P. M. In *The Fifth International Conference on Gas Hydrates*: Trondheim, Norway, 2005; Vol. 1, pp 317−321.
(13) Koh, C. A.; Westacott, R. E.; Zhang, W.; Hirachand, K.; Creek, J. L.; Soper, A. K. *Fluid Phase Equilib.* **2002**, *194*, 143−151.
(14) Storr, M. T.; Rodger, P. M. In *Ann. N. Y. Acad. Sci.* **2000**, *912*, 669−677.
(15) Makogon, T. Y.; E. Dendy Sloan, J. In *Fourth International Conference on Gas Hydrates*; Yokohama, Japan, 2002; pp 498−503.
(16) Zeng, H.; Wilson, L. D.; Walker, V. K.; Ripmeester, J. A. *Can. J. Phys.* **2003**, *81*, 17−24.
(17) Hutter, J. L.; King, H. E.; Lin, M. Y. *Macromolecules* **2000**, *33*, 2670−2679.
(18) Makogon, T. Y.; Larsen, R.; Knight, C. A.; Sloan, E. D. *J. Cryst. Growth* **1997**, *179*, 258−262.
(19) Larsen, R.; Knight, C. A.; Sloan, E. D. *Fluid Phase Equilib.* **1998**, *151*, 353−360.
(20) Sakaguchi, H.; Ohmura, R.; Mori, Y. H. *J. Cryst. Growth* **2003**, *247*, 631−641.
(21) Christiansen, R. L.; Sloan, E. D. *Int. Conf. Nat. Gas Hydrates* **1994**, *715*, 283−305.
(22) Sloan, E. D.; Fleyfel, F. *AIChE J.* **1991**, *37*, 1281−1292.
(23) Kvamme, S. *Ann. N. Y. Acad. Sci.* **2000**, *912*, 496−501.

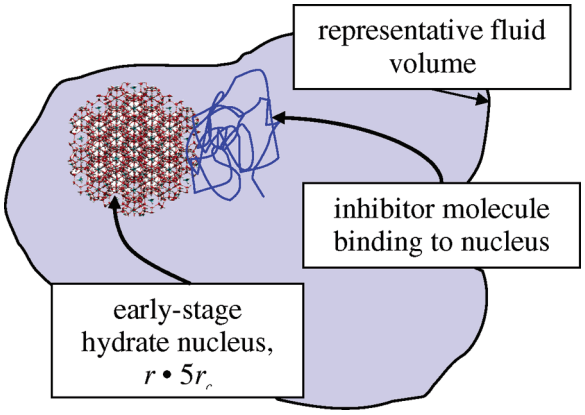

Figure 3. Conceptual model for inhibitor binding and crystal growth inhibition. Shown is step one of the two-step mechanism for hydrate inhibition. Inhibitor molecules disrupt the local organization of water and guest molecules and attach to forming hydrate nuclei, transferring enthalpy locally into the nuclei.

sizes of nuclei are on the order of tens of angstroms.[8,24] On the other hand, the distance between inhibitor molecules is much larger than that. We can illustrate this using poly(*N*-vinyl-2-caprolactam), called PVCap, with a molecular weight of ~100,000. PVCap at approximately this molecular weight has been measured using small-angle neutron scattering to have a radius of gyration, R_g, of 155 Å[25] and is highly miscible in water at temperatures of interest ($T_{cloud} \approx 30$ °C). If PVCap is added to water at 0.5 wt %, its approximate volume fraction is 0.4%. Assuming that the PVCap polymers are evenly dispersed throughout the water phase, then their approximate average separation would be 300 Å. Thus, nuclei could still form.

Given the information summarized briefly above, we propose that hydrate inhibition occurs via a two-step mechanism. (1) Inhibitor molecules disrupt the local organization of the water and guest molecules, increasing the barrier to nucleation and nuclei propagation (Figure 3). (2) Once nucleation occurs, the inhibitor binds to the surface of the hydrate nanocrystal and retards further growth along the bound growth plane (Figure 4).

In the first step, the disruption of newly forming nuclei occurs as proposed by Storr et al.[11] who used simulations and demonstrated that localized structure inconsistent with hydrate formation was induced by tributylammoniumpropylsulfonate (TBAPS) over several solvation shells. This element of the mechanism hitherto has not been verified experimentally. Our work focuses on step (2), and as we will demonstrate, step (2) is consistent with several qualitative experimental results.

While TBAPS was shown to have an inhibition activity comparable to poly(*N*-vinyl-2-pyrrolidone), known as PVP, the resulting crystal morphology was quite different. PVP and PVCap have been shown to result in platelike hydrate crystals upon crystallization,[11,18−20] consistent with part (2) of the proposed mechanism whereas the hydrate crystals grown in the presence of TBAPS have been observed to be deformed, and particularly elongated, octahedra.

Once an inhibitor molecule such as PVP binds to one face of the hydrate nanocrystal, growth along that face is slowed significantly. King et al.[25] have shown that in the presence of a hydrate-crystal/liquid slurry three active inhibitors, PVP, PVCap, and *N*-methyl,*N*-vinylacetamide/*N*-vinyl-2-caprolactam copolymer (VIMA/PVCap), are adsorbed to the hydrate-crystal surface while a noninhibiting polymer, poly(ethylene oxide) was not adsorbed, further supporting the surface binding hypothesis. Given these initial results, *we hypothesize that the stronger its binding to the hydrate surface, the more disruptive an inhibitor is to the structure of forming hydrate nuclei*. The rest of this paper presents the test of this hypothesis using qualitative experimental results from the literature and new quantitative molecular computational results.

Methodology

Our approach is different from that of previous studies[11,12,26−30] with four key variations: the use of a liquid water phase in equilibrium with the hydrate crystal, the quantitative analysis of the energetics of inhibitor binding, the use of fully dynamic water molecules in the hydrate crystal, and the placement of the water-soluble inhibitor in the liquid water phase as opposed to placement in the gas or vacuum phase. Previous computational studies focused on the morphologic effects,[11] the topology[26−29] of the hydrate−inhibitor interaction, or the structural behavior of inhibitor molecules in solution,[30] all structural studies. This project focuses on estimating the binding energy of the inhibitor on the hydrate crystal surface.

Development of Molecular-Interaction Parameters. Hydrate clathrates cannot be modeled quantitatively on a molecular level without incorporating accurate guest−host interactions. Our guest−host potentials are derived from ab initio calculations and are directly connected to molecular force interactions and sizes and proven to reproduce experimental data for the hydrate-clathrate system.[31−33] In this study, we have developed and parametrized an accurate potential for methane−water interactions that can be used with the CHARMM molecular dynamics package. This was developed using our ab initio methane−water potential energy surface developed earlier.[31,34] The 18,000 methane−water ab initio energies were fit to the CHARMM potential, minimizing the Boltzmann-weighted square error χ between the ab initio potential energy surface and the CHARMM potential energy surface.

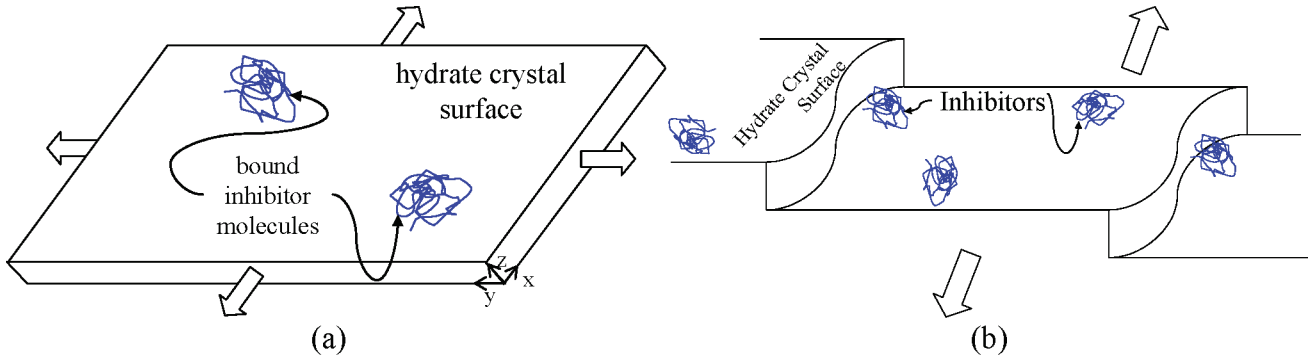

Figure 4. Conceptual model for inhibitor binding and crystal growth inhibition. Shown is step two of the two-step mechanism for hydrate inhibition. (a) Once the crystal has nucleated and crystal growth begins, the inhibitor binds to the surface and retards growth in the *z*-direction by hindering step growth through the process of step-pinning (b).

$$\chi = \sum_{i}^{\text{no. of QM points}} \left[\exp\left(\frac{-\Delta E_{\text{cp},i}}{kT}\right)_{\text{QM}} - \exp\left(\frac{-\Phi_i^{\text{tot}}}{kT}\right)_{\text{model}} \right]^2$$

with:

$$\Phi^{\text{tot}} = \sum_{k}^{\text{no. of sites}} \Phi_{\text{CH}_4-k} \qquad (1)$$

The adjustable parameters in the CHARMM potential are the characteristic energy, ϵ, and the soft core radius, σ, of the L-J 6-12 potential for both the $H_4\mathbf{C}-\mathbf{O}H_2$ and the $H_3C\mathbf{H}-\mathbf{O}H_2$ interactions as shown in Figure 5. (The atoms marked in bold indicate the location of the interaction site for use in a site−site potential.) Interaction parameters given in Tables 1 and 2 were found by applying traditional Lorentz−Berthelot mixing rules:

$$\epsilon_{ij} = \sqrt{\epsilon_i \epsilon_j}$$
$$\sigma_{ij} = \frac{\sigma_i + \sigma_j}{2} \qquad (2)$$

The CHARMM model with this set of intermolecular potential parameters was then verified by simulation of a 34.6 Å cubic volume consisting of eight structure II (sII) unit cells (2 × 2 × 2) with full methane occupancy (see Figure 6). This scale results in a simulation with 1088 water and 192 methane molecules. The TIP4P model was used for water in the development of the methane potential and in the dynamic simulations. The sII crystal was then simulated using CHARMM until the simulation reached equilibrium, and then molecular dynamics were run for 100 ps. During the sII hydrate simulation the lattice parameter of the sII hydrate unit cell ranged from 17.16 to 17.45 Å with an average of 17.31 Å and a standard deviation of 0.022 Å. This result compares favorably to the experimental lattice parameter of 17.3 Å and serves as a validation of the use of our developed methane−water potential in these dynamic simulations.

Structure II Hydrate Surface. A molecular-scale slab model was used in surface-interaction calculations involving the sII hydrate molecules and inhibition molecules. The hydrate molecules are embedded in a particular crystallographic plane that spans four sII unit cells placed in a 34.6 Å × 34.6 Å × 17.3 Å box. On top of the solid layer of crystalline hydrate is placed a layer of liquid water another 17.3 Å thick. To replicate conditions occurring in gas transmission line hydrate crystal growth, the liquid layer serves as the water condensate layer that solubilizes the inhibitor molecules. Figure 7 shows the resulting 34.6 Å cubic simulation box. Periodic boundary conditions were incorporated to model the solid−liquid system dynamically and to simulate a stable hydrate crystal surface at 200 K and 4 bar.

Determination of Inhibitor Binding Energy. Once the hydrate crystal−liquid water slab model described above was constructed, a monomer unit of inhibitor was placed in either the middle of the liquid phase or near the hydrate solid surface. We define the surface adsorption energy as the difference between the energy of the entire simulation with the monomer bound to the crystal minus the energy of the system with the monomer in the bulk liquid. NPT molecular dynamic simulation runs were then performed on the bound and unbound systems for 6−7 ns, allowing full ranges of motion for all molecules. The inhibitor molecules we studied were PVP, PVCap, *N*-methyl,*N*-vinylacetamide (VIMA), and PEO, a noninhibitor,[25] see Figure 8 for a description of their molecular structures.

Inhibitor Molecules Studied. The partial atomic charges for PVP, PVCap, *N*-methyl,*N*-vinylacetamide, and PEO were calculated using Gaussian 03, and the nonbonded interaction parameters were chosen from the parameters optimized for alkanes found in CHARMM. In this

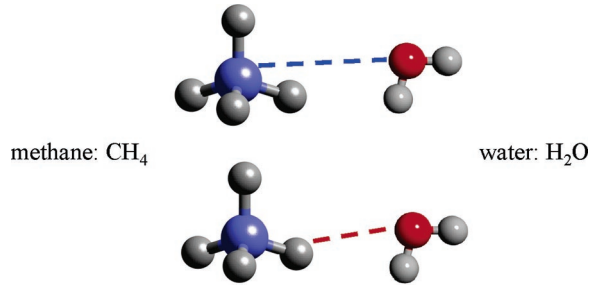

Figure 5. Site−site interactions between methane (C = blue, H = gray), and water (O = red, H = gray). Accounted for in the developed CHARMM potential.

Table 1. CHARMM Potential Parameters Determined for the Methane−Water Interaction (atoms marked in bold indicate interaction site)

interaction	$\epsilon_{C,H-O}$ (kcal/mol)	$\sigma_{C,H-O}$ (Å)	$Q_{C,H,O}$ (e)	Q_M (e)
$H_4\mathbf{C}-\mathbf{X}$	0.18	3.5	−0.24	
$H_3C\mathbf{H}-\mathbf{X}$	0.03	2.5	0.06	
TIP4P[35,36] $H_2\mathbf{O}-\mathbf{O}H_2$	0.155	3.154	0.52	−1.04

Table 2. OPLS[37,38] Potential Parameters Commonly Used for Methane (atoms marked in bold indicate interaction site)

site	ϵ_{ij} (kcal/mol)	$\sigma_{C,H-O}$ (Å)	$Q_{C,H}$ (e)
$H_4\mathbf{C}-\mathbf{X}$	0.066	3.5	−0.24
$H_3C\mathbf{H}-\mathbf{X}$	0.030	2.5	0.06

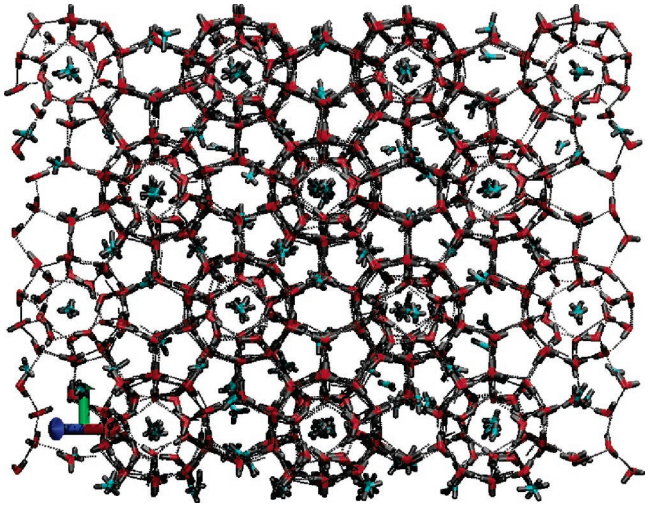

Figure 6. 34.6 Å cubic simulation box consisting of eight structure II unit cells with methane guest molecules.

(24) Larson, M. A.; Garside, J. *Chem. Eng. Sci.* **1986**, *41*, 1285−1289.
(25) King, H. E.; Hutter, J. L.; Lin, M. Y.; Sun, T. *J. Chem. Phys.* **2000**, *112*, 2523−2532.
(26) Carver, T. J.; Drew, M. G. B.; Rodger, P. M. *J. Chem. Soc., Faraday Trans.* **1995**, *91*, 3449−3460.
(27) Carver, T. J.; Drew, M. G. B.; Rodger, P. M. *J. Chem. Soc., Faraday Trans.* **1996**, *92*, 5029−5033.
(28) Kvamme, B.; Huseby, G.; Forrisdahl, O. K. *Mol. Phys.* **1997**, *90*, 979−991.
(29) Carver, T. J.; Drew, M. G. B.; Rodger, P. M. *Ann. N. Y. Acad. Sci.* **2000**, *912*, 658−668.
(30) Carver, T. J.; Drew, M. G. B.; Rodger, P. R. *Phys. Chem. Chem. Phys.* **1999**, *1*, 1807−1816.
(31) Cao, Z. T.; Tester, J. W.; Trout, B. L. *J. Chem. Phys.* **2001**, *115*, 2550−2559.
(32) Anderson, B. J.; Tester, J. W.; Trout, B. L. *J. Phys. Chem. B* **2004**, *108*, 18705−18715.
(33) Cao, Z. T.; Tester, J. W.; Sparks, K. A.; Trout, B. L. *J. Phys. Chem. B* **2001**, *105*, 10950−10960.
(34) Anderson, B. J.; Tester, J. W.; Trout, B. L. *J. Phys. Chem. B* **2004**, *108*, 18705−18715.

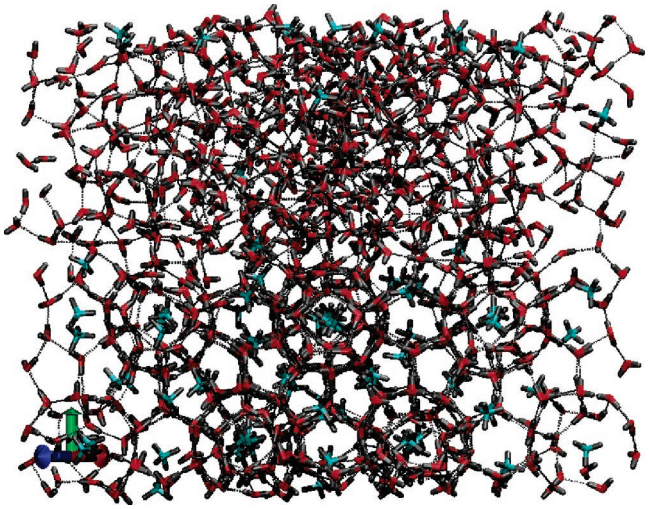

Figure 7. Hydrate slab with liquid water in the fluid phase.

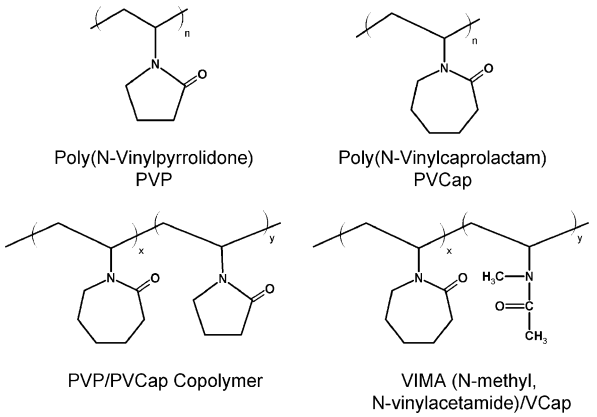

Figure 8. Structure of four common kinetic hydrate inhibitors comprised of the monomer units studied in this project.

study we assumed that the binding energy of the monomer was independent of the chain length and was linearly additive. Therefore, the PVP/PVCap copolymer is analyzed by considering both the PVP and PVCap monomer units as well as the VIMA/VCap polymer examined by King et al.[25] This assumption is justified in the work by Lederhos et al.[7] which showed that PVP/PVCap copolymers exhibited induction times for hydrate formation between that of the two homopolymers.

Free Energy of Binding. The Gibbs free energy of binding is calculated using Kirkwood's coupling parameter method.[39] Specifically, it is the difference in the Gibbs free energy of inserting an inhibitor molecule on the surface of the hydrate and in the liquid water phase. Because binding energy is a thermodynamic property, the insertion of an inhibitor can be performed along a fictitious pathway λ, in which λ = fraction of insertion. To be able to evaluate a relatively smooth energy profile from an unincorporated (ghost) inhibition molecule (invisible to other molecules) at $\lambda = 0$ to a fully incorporated inhibition molecule at $\lambda = 1$, we have used 10 evenly spaced values of λ over λ [0,1] in our energy simulations. λ is used as a multiplier on the ϵ value in the nonbonded energy terms between any atom on the inhibitor and the other molecules in the simulation, effectively turning on and off the inhibitor−water and inhibitor−methane interactions. To calculate the free energy, the Hamiltonian, $\mathcal{H}$, is calculated for each value of λ and integrated from $\lambda = 0$ to $\lambda = 1$ as shown below:[40]

$$G(\lambda = 1) - G(\lambda = 0) = \int_0^1 \left\langle \frac{\mathrm{d}\mathcal{H}(\lambda)}{\mathrm{d}\lambda} \right\rangle_\lambda \mathrm{d}\lambda \cong \int_0^1 \langle \mathcal{H}_1 - \mathcal{H}_0 \rangle_\lambda \mathrm{d}\lambda \quad (3)$$

where $\mathcal{H}(\lambda) = \mathcal{H}_0 + \lambda(\mathcal{H}_1 - \mathcal{H}_0)$, and G is the Gibbs free energy.

Estimation of Statistical Error. Determination of the variances of the ensemble averages of the system energy not only allows us to calculate potential error in the values for system energy but also provides a metric for determining the length of simulation required to calculate accurate statistical quantities.

The reported error bars for the energy calculations are the standard deviations of the ensemble average energy and were calculated using both the method described by Frenkel and Smit[40] in Appendix D and the method developed by Flyvbjerg and Petersen[41] as follows. The ensemble average is estimated from

$$\langle E \rangle \approx \bar{E} \equiv \frac{1}{L}\sum_{i=1}^{L} E_i \quad (4)$$

where $E_1, E_2, ..., E_L$ are consecutive values of the energy of the system over windows of simulation with length L, assuming all discrete E_i values have been taken after the system reaches equilibrium. The variance is estimated by

$$\sigma^2(E) = \langle E^2 \rangle - \langle E \rangle^2 \approx \frac{1}{L}\sum_{i=1}^{L} [E_i - \bar{E}]^2 \quad (5)$$

One now needs to eliminate correlation effects due to the consecutive nature of molecular dynamic simulations. To do this, the energy is grouped into consecutive blocks, computing the average along the way. The block averages will exhibit less correlation as the blocking continues.

$$E_i' = 0.5(E_{2i-1} + E_{2i}) \quad (6)$$

So now $L' = 0.5\ L$, and the variance of the new set is

$$\sigma^2(E') = \langle E'^2 \rangle - \langle E' \rangle^2 \approx \frac{1}{L'}\sum_{i=1}^{L'} E_i'^2 - \bar{E}'^2 \quad (7)$$

As the blocking procedure is followed, we can find our estimate of the variance as

$$\sigma^2(E) \approx \frac{\sigma^2(E')}{L' - 1} \approx \text{constant} \quad (8)$$

Results/Discussion

Energetics of Binding. The optimal binding site for both the PVP and PVCap monomers on the hydrate surface was found to be a partially formed 16-sided hexakaidecahedron ($5^{12}6^4$) as shown in Figure 9a and c. On the plane chosen to create the surface of the hydrate, the hexakaidecahedron is cleaved in half, leaving the open top side exposed to the liquid phase. The PVP monomer binds in this half-cavity on the hydrate surface with an energy of binding of -20.6 ± 2.5 kcal/mol. The ensemble-averaged energy of PVP on and off the hydrate surface resulting from the MD simulation is shown in Figure 10. The system equilibrated in about 2.5 ns, and then

(35) Jorgensen, W. L.; Chandrasekhar, J.; Madura, J. D.; Impey, R. W.; Klein, M. L. *J. Chem. Phys.* **1983**, *79*, 926−935.
(36) Jorgensen, W. L.; Madura, J. D. *Mol. Phys.* **1985**, *56*, 1381−1392.
(37) Jorgensen, W. L.; Severance, D. L. *J. Am. Chem. Soc.* **1990**, *112*, 4768−4774.
(38) Kaminski, G.; Duffy, E. M.; Matsui, T.; Jorgensen, W. L. *J. Phys. Chem.* **1994**, *98*, 13077−13082.
(39) Kirkwood, J. G. *J. Chem. Phys.* **1935**, *3*, 300−313.
(40) Frenkel, D.; Smit, B. *Understanding molecular simulation: from algorithms to applications*, 2nd ed.; Academic Press: San Diego, 2002.
(41) Flyvbjerg, H.; Petersen, H. G. *J. Chem. Phys.* **1989**, *91*, 461−466.

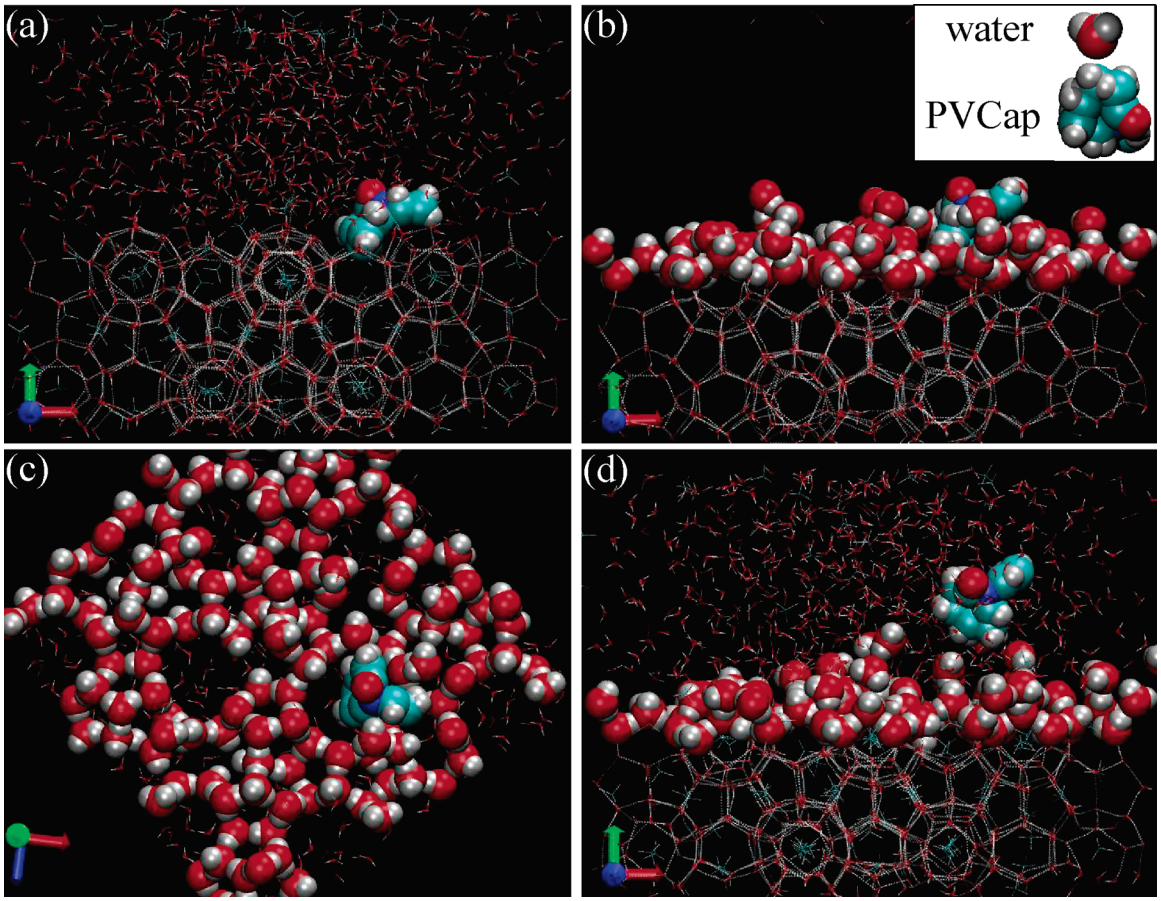

Figure 9. Snapshots from the simulation of PVCap in the presence of a hydrate surface. (a) PVCap monomer adsorbed into the open face of a hexakaidecahedron. Hydrogen bonds are shown in white to illustrate the hydrate lattice. (b) Liquid waters found in frame (a) have been removed, whereas the waters on the surface of the hydrate crystal are expanded in size to their van der Waals radii to illustrate the surface structure. (c) Hydrate surface rotated toward the reader to show the binding site of the PVCap monomer. (d) PVCap monomer away from the surface of the hydrate.

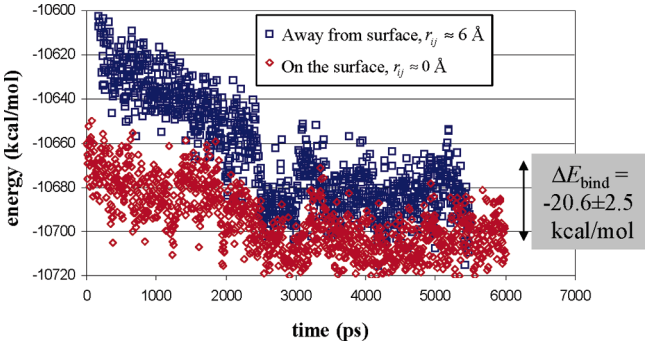

Figure 10. Dynamic energy of the PVP−hydrate surface.

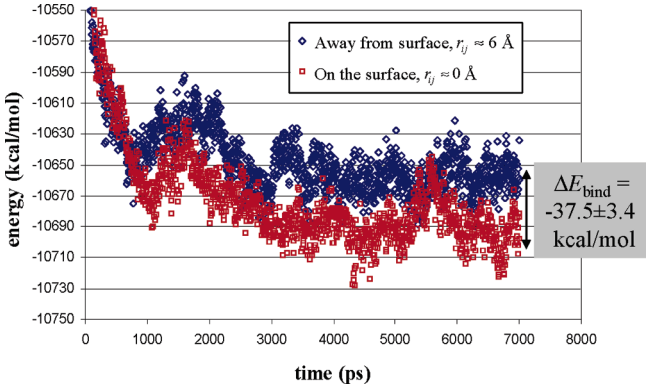

Figure 11. Dynamic energy of the PVCap−hydrate surface.

statistics were accumulated for another 3−4 ns where each time step was 0.001 ps. Similarly, as illustrated in Figure 11 the energy of binding of PVCap was found to be −37.5 ± 3.4 kcal/mol. PVCap, therefore, is clearly the stronger binder to the hydrate crystal surface. The energy of binding to the hydrate surface for PVCap is about 20 kcal/mol stronger than the energy of binding of PVP.

The free energy calculation for PVCap is shown in Figure 12. The free energy of binding for PVCap is calculated to be −9.4 ± 3.8 kcal/mol, whereas the free energy of binding of PVP is found to be 0.5 ± 3.7 kcal/mol. The free energy of binding of PVP is effectively zero, while the equilibrium reaction for PVCap binding favors the inhibitor bound to the hydrate surface as opposed to in solution. In the case of PVP, the negative binding energy coupled with the neutral (zero) binding free energy can be interpreted as an exothermic phase adsorption reaction in which an equal number of PVP species bind to and dissociate from the hydrate surface at equilibrium.

The PVCap binding event is also exothermic ($\Delta E < 0$); however, in the case of PVCap binding, the equilibrium is shifted toward "products" (bound species) by the negative free energy of binding. Therefore, a higher fraction of PVCap monomers are bound to the surface compared to PVP. This is consistent with the relative effectiveness of these two inhibitors found experimentally, our proposed mechanism, and with the low fraction of bound PVP species found by Hutter et al.[17]

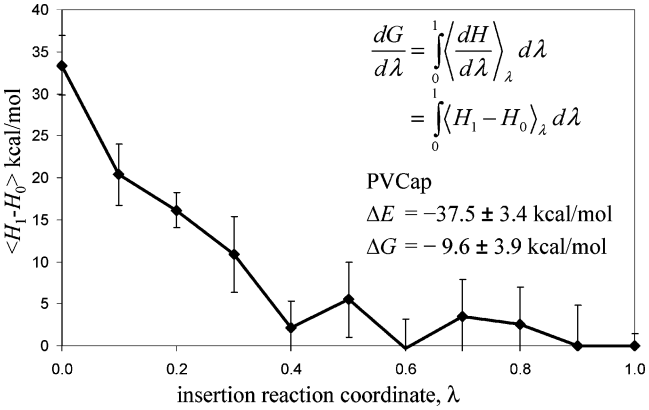

Figure 12. Differential Hamiltonion plot for PVCap.

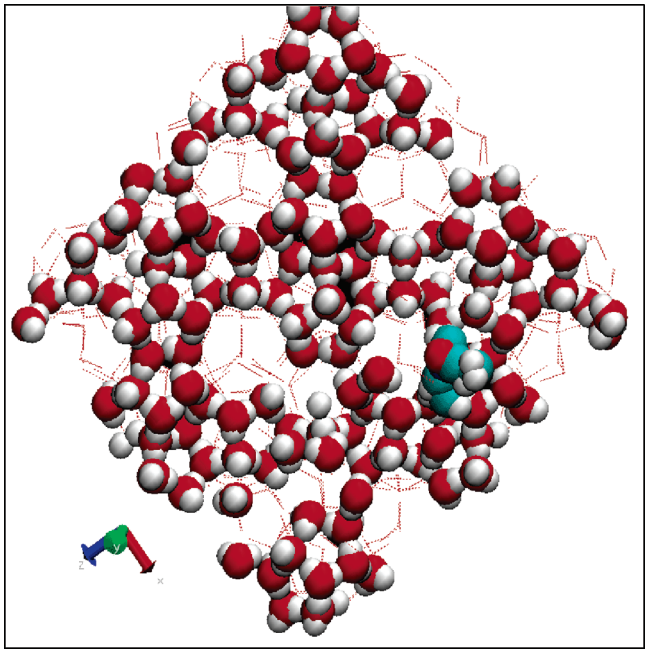

Figure 13. VIMA bound to the sII hydrate surface in the minimum-energy binding site.

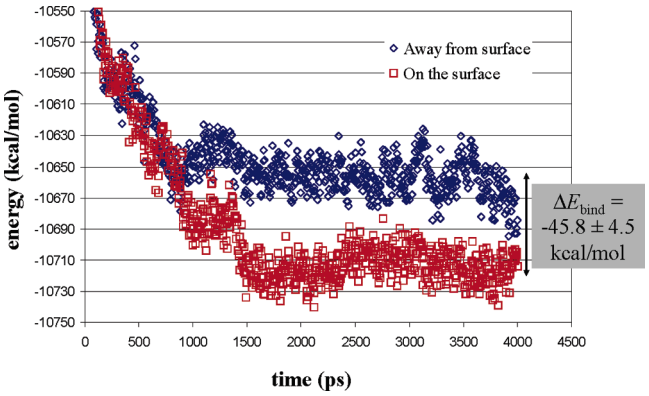

Figure 14. Dynamic energy of the VIMA−hydrate surface.

The lowest-energy binding site for the VIMA monomer is significantly different from that for the two previous inhibitor monomers, PVP and PVCap. As shown in Figure 13, in contrast to the binding site found for PVP and PVCap (in the half-formed hexakaidecahedron cavity) the VIMA monomer binds to what one might call a "bridge" site between two adjacent cavities. In the MD simulation, the VIMA monomer jumped from the higher-energy binding site inside the open cavity to the bridge site, thus lowering its total energy. This transition corresponds to the second drop in ensemble energy occurring around 1400 ps as seen in Figure 14. The resulting binding energy for the VIMA monomer is -45.8 ± 4.5 while the binding free energy is -15.1 ± 4.6, both significantly lower than the binding energy and free energy for the PVP and PVCap monomers.

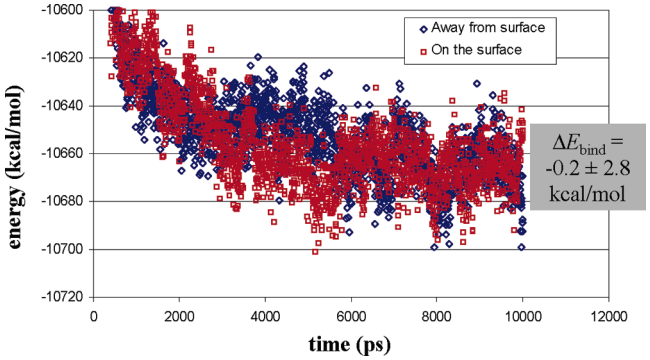

Figure 15. Dynamic energy of the PEO−hydrate surface.

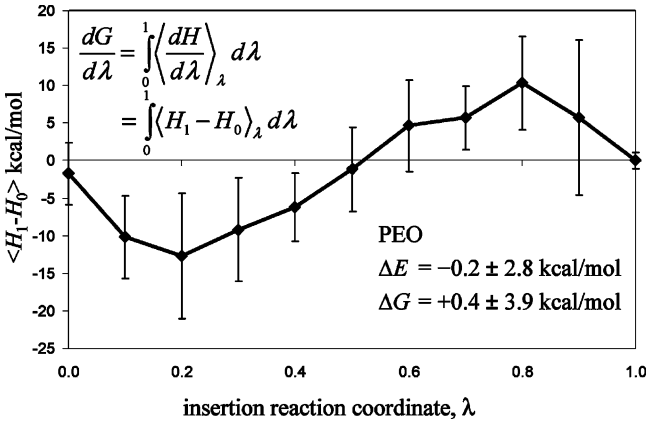

Figure 16. Differential Hamiltonion plot for PEO.

Table 3. Summary of Binding Energies for Four Monomers Studied[c]

Molecule	ΔE (kcal/mol)	ΔG (kcal/mol)	$T\Delta S$ (kcal/mol)	excess low-q scattering[25] (cm^{-1})[a]	Increasing inhibitor effectiveness[7,25,42,43]
PEO	-0.2 ± 2.8	+0.4 ± 3.9	-0.6	0	↓
PVP	-20.6 ± 2.5	+0.5 ± 3.7	-21.1	3	
PVCap	-37.5 ± 3.4	-9.4 ± 3.8	-28.1	10	
VIMA	-45.8 ± 4.5	-15.1 ± 4.6	-30.7	37[b]	

[a] Excess low-q scattering used as a measure of the change in polymer conformation due to the introduction of hydrate surfaces for binding. This value is interpreted as a measure of the degree of polymer binding on the hydrate surfaces. [b] Excess low-q scattering measured for VIMA/PVCap copolymer. King et al.[25] state that VIMA/PVCap is the most effective inhibitor. [c] Inhibitor effectiveness increases in the direction of the arrow.

The binding energy and free energy for PEO was calculated as a control experiment. King et al.[25] concluded from their small-angle neutron scattering (SANS) study that "there is no evidence of an adsorbed layer" of PEO in the presence of hydrate surfaces. This result is consistent with our proposed mechanism in that if there is no polymer adsorption on the hydrate surfaces then there would be no hydrate formation inhibition. In our MD simulations, we also observe adsorption of PEO to the surface of hydrate crystals. The resulting "binding energy" for PEO is

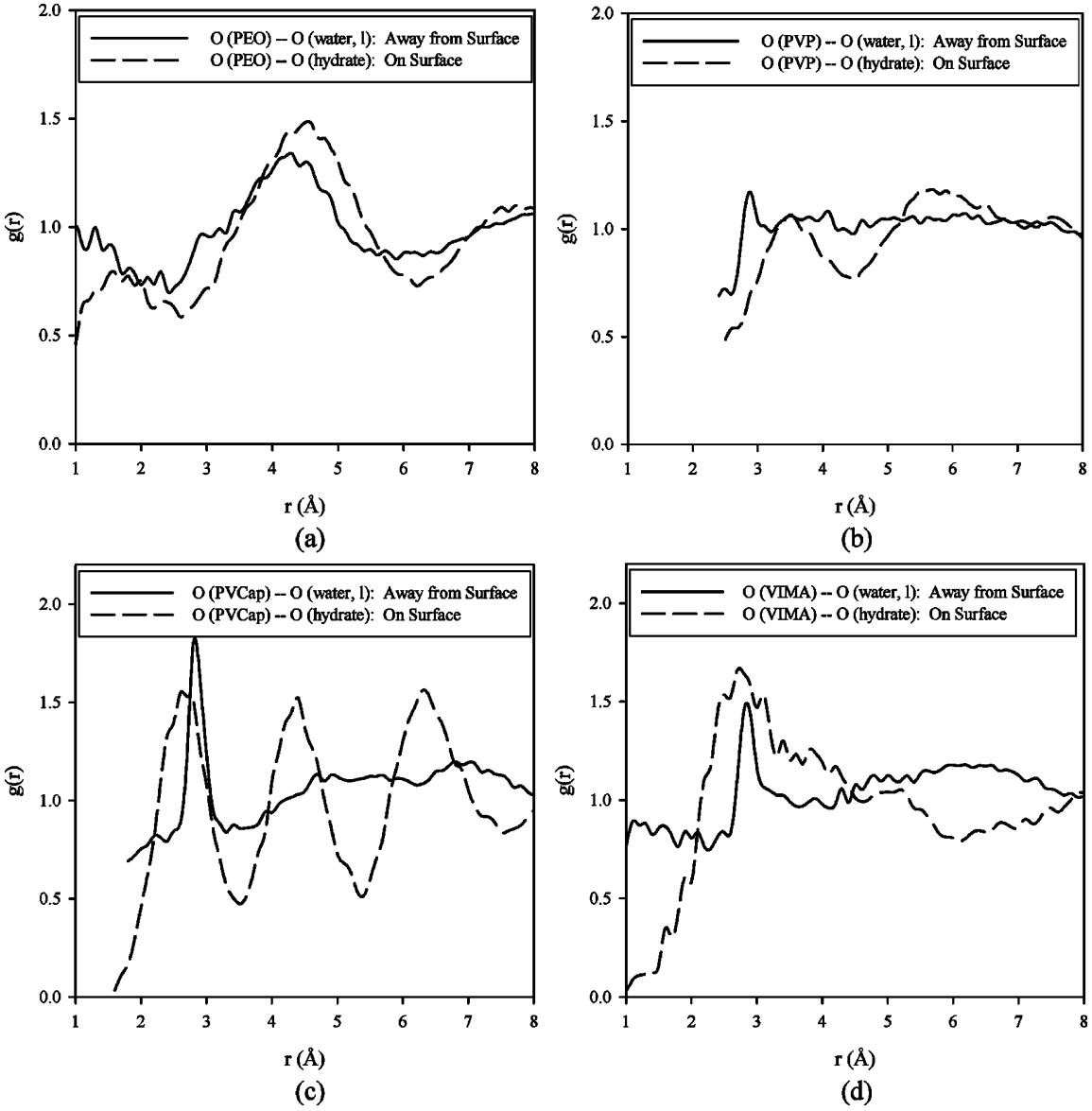

Figure 17. Radial distribution functions between the double-bonded oxygen on (a) PEO, (b) PVP, (c) PVCap, and (d) VIMA and the oxygen on water when the monomer is bound to the hydrate surface and away from the surface. Differences illustrate the effect of the hydrate surface on the morphology of the monomer and surrounding waters.

-0.2 ± 2.8 (Figure 15), and the binding free energy (Figure 16) is $+0.4 \pm 3.9$, indicating that the binding event is not thermodynamically favorable. Table 3 summarizes the binding energy study for the four molecules examined and compares the binding energy and free energy to the reported effectiveness of the inhibitors. The rightmost column in Table 3 shows the order of increasing inhibitor effectiveness as described by a number of different research and engineering groups.[7,25,42,43] Inhibitor effectiveness ranges from inactive (PEO) to very active (VIMA/VCap).[25]

Binding and Surrounding Water Structure. Structural effects were examined by calculating the radial distribution functions, $g(r)$, of the double-bonded oxygen on the inhibitor molecules with the oxygen of water in either the hydrate phase (bound inhibitor) or the liquid phase (unbound).

$$g(r_{ij}) = \frac{V}{N^2}\langle\delta(r - r_{ij})\rangle \qquad (9)$$

where i is the oxygen on the inhibitor molecule and j is the oxygen in water in either the hydrate or liquid phase (indicated on plots). V/N^2 normalizes the $g(r)$ relative to an ideal gas of the same density. Figure 17 shows the radial distribution functions, RDFs, between the oxygen on the monomer and the oxygen on the surrounding water molecules for monomers both on and off the hydrate surface. One can clearly see in Figure 17a that the hydrate surface has little effect on the PEO monomer since the $g(r)$ does not change significantly. One should expect this result both from the SANS results[25] and the energetic results from our simulation. One can also see a noticeable increase in the interaction between the monomer and the hydrate surface in Figure 17b−d. PVP, Figure 17b, is affected slightly, whereas PVCap and VIMA, Figure 17c,d, are strongly affected. Note that there is a strong oxygen−oxygen correlation for both PVCap and VIMA on and off the surface.

(42) Sloan, E. D. *Clathrate hydrates of natural gases*, 2nd ed.; Marcel Dekker: New York, 1998.
(43) Freer, E. M.; Sloan, E. D. *Ann. N. Y. Acad. Sci.* **2000**, *912*, 651−657.

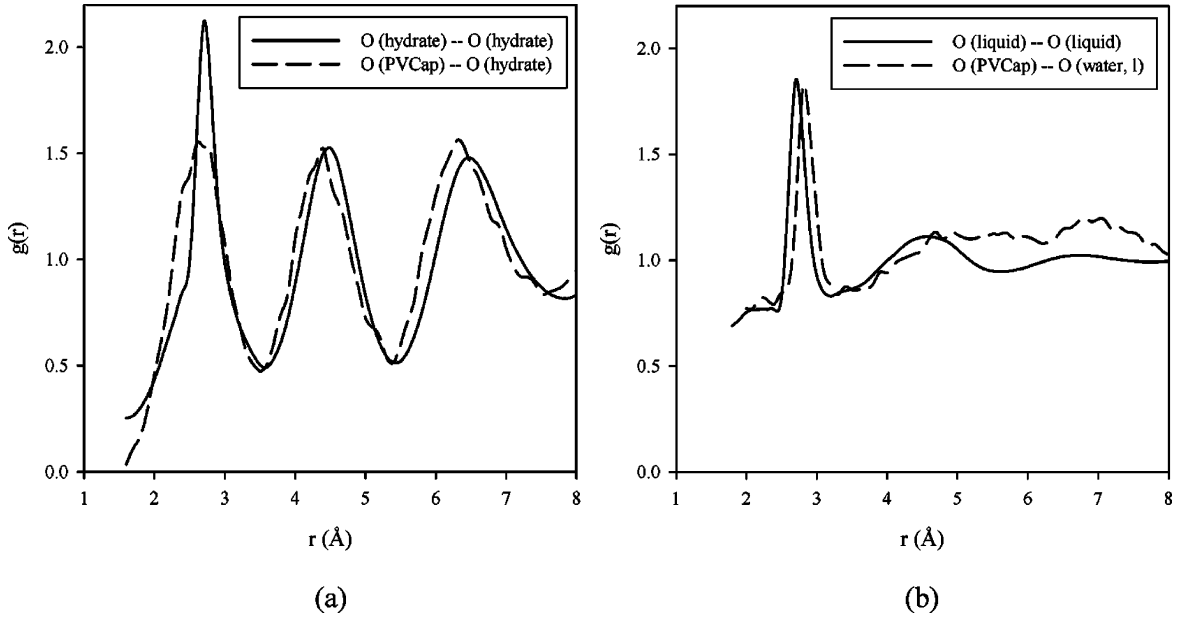

Figure 18. Radial distribution functions between the double-bonded oxygen on PVCap and the oxygen on water when the PVCap is (a) bound to the hydrate surface and (b) in solution away from the hydrate surface.

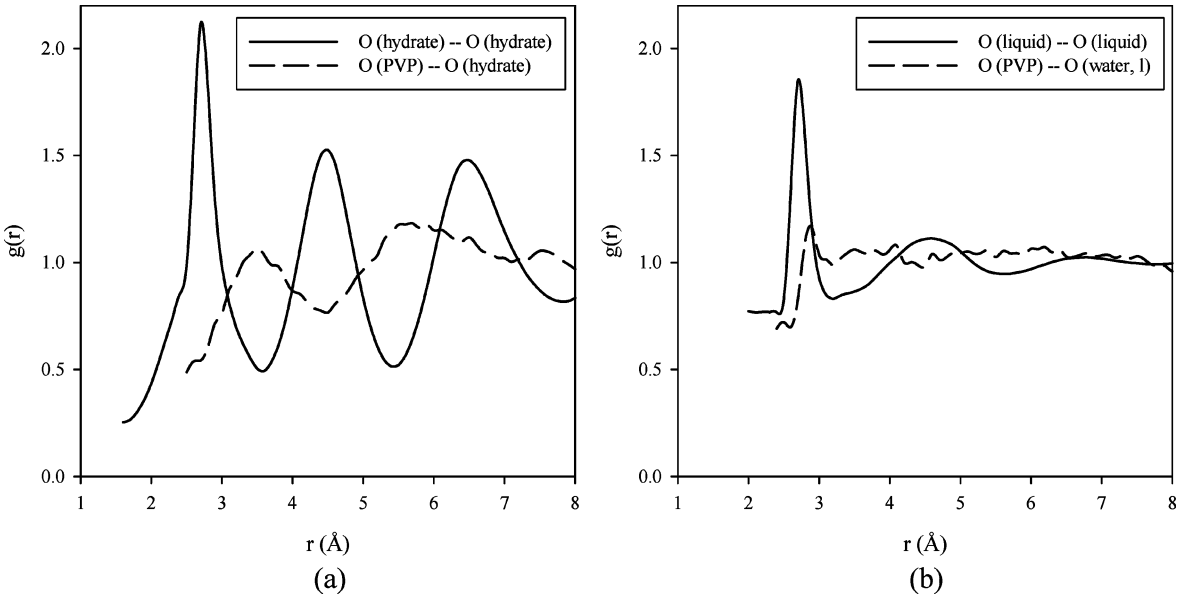

Figure 19. Radial distribution functions between the double-bonded oxygen on PVP and the oxygen on water when the PVP is (a) bound to the hydrate surface and (b) in solution away from the hydrate surface.

To examine more closely the water−inhibitor interaction, we look at oxygen−oxygen RDFs for monomer−water interactions and compare them to $H_2\mathbf{O}-\mathbf{O}H_2$ RDFs. This way one can examine both how the monomer fits into the water structure and how it affects the water structure. The $g(r)$ of PVCap, Figure 18, shows a great deal of correlation between the oxygen on the PVCap and the oxygen on the hydrate and liquid waters. The double-bonded oxygen falls into a lattice position typically occupied by a water molecule, thus leading to the strong energy of binding and the favorable free energy of reaction. In the liquid water phase, this ═O is also coordinated in such a manner as to act like a water molecule.

The calculated $g(r)$ of PVP, Figure 19, does not show the strong correlation with the hydrate crystal that the $g(r)$ of PVCap does. In fact, the first water oxygen neighbor is shifted away from the double-bonded oxygen in both the surface bound (a) and liquid water (b) cases. As evident in Figure 19b, the PVP monomer has little effect on the structure of water in the surrounding area. Finally, one can see from the $g(r)$ of VIMA, Figure 20a, that there is strong correlation in the first water shell both on and off the hydrate surface; however, unlike PVCap, the subsequent shells do not exhibit strong correlation. This is due to the double binding site nature of the VIMA monomer discussed in more detail in the next section. VIMA has two possible binding sites, between which the monomer frequently switches. These binding sites are not identical when bound to the hydrate surface (only one is bound at a time), and therefore the O−O $g(r)$ is averaged between these two distances, widening the first coordination shell and smoothing out the subsequent shells. Furthermore, as evident in Figure 20b, VIMA interacts strongly with the water in the liquid solution, where

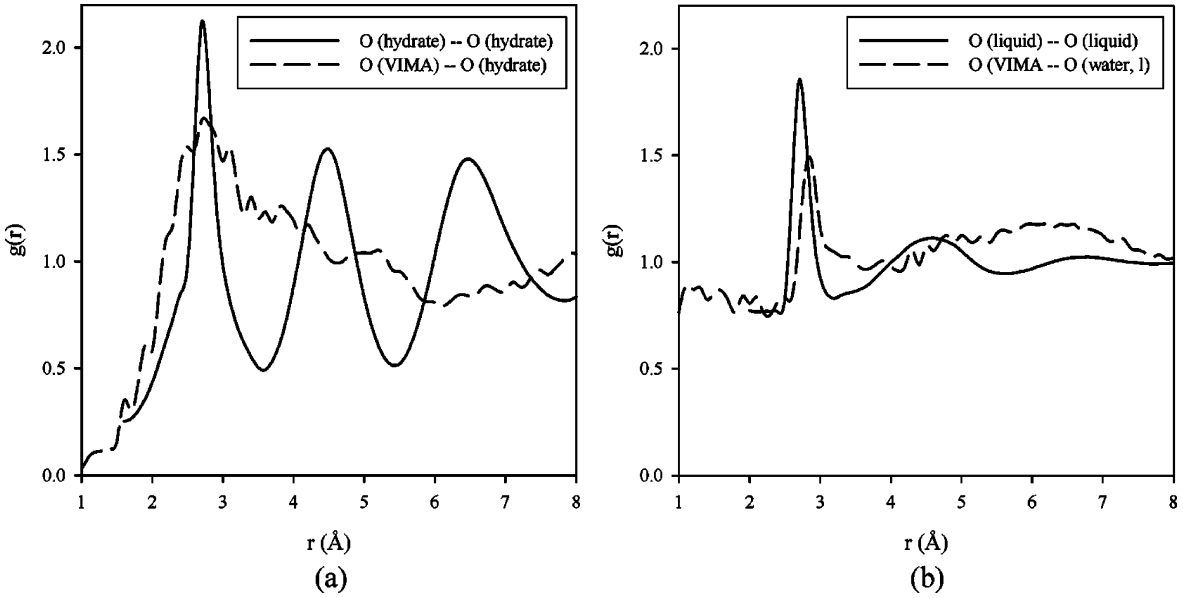

Figure 20. Radial distribution functions between the double-bonded oxygen on VIMA and the oxygen on water when the VIMA is (a) bound to the hydrate surface and (b) in solution away from the hydrate surface.

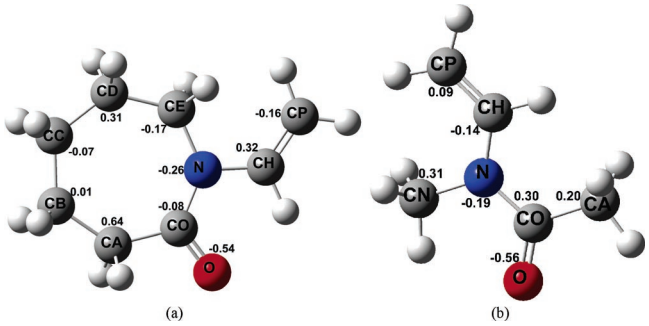

Figure 21. Partial charges on (a) PVCap and (b) *N*-methyl,*N*-vinylacetamide. Labels on atoms are simply to differentiate atoms of the same type from one another. For labels with two capital letters the first letter is the atom type, and the second letter is to label that atom.

liquid water molecules surround the monomer, making the oxygen sites appear more similar.

Molecular Characteristics Favoring Inhibition. From our molecular simulations, we have been able to identify two molecular characteristics that lead to the strong binding of PVCap: (1) a charge distribution on the edge of the PVCap (from O to CA in Figure 21a) that mimics the charge separation in the water molecules on the surface of the hydrate and (2) the congruence of the size of the PVCap with respect to the available space at the tetrakaidecahedron binding site. VIMA has been shown to have an inhibitor effect even stronger than PVCap and exhibits a similar charge distribution (see Figure 21b). However, unlike PVCap, there are two partially positive carbons (labeled CA and CN in Figure 21b) that double the opportunity for alignment with water to form hydrogen bonds.

PVP has a charge distribution similar to that of PVCap, thus allowing PVP to form hydrogen bonds with the waters on the hydrate surface. However, the size of the PVCap ring proves to be much more conducive to strong binding than that of the small PVP ring. When PVCap is bound in the open cage, its molecular motion is limited much more than the motion of the PVP monomer. The RMSD of the PVCap monomer is 1.155 Å, while that of PVP is 2.466 Å, both over a period of 3 ns. More specifically, the atoms CO and CA on PVCap have respective RMSDs of 0.509 and 0.659 Å, while the equivalent atoms on PVP have respective RMSDs of 0.844 and 2.390 Å, demonstrating that the motion of the carbon with the double-bonded oxygen (labeled CO) and its adjoining carbon (labeled CA), the bonding side of the ring, is much more restricted for PVCap compared to that for PVP. Therefore, the characteristics of this side of the ring should govern the strength of the binding interaction.

Conclusions

Within we propose and test a two-fold mechanism for hydrate inhibition by four inhibitor molecules (PEO, PVP, PVCap, and VIMA) using molecular simulations. The mechanism hypothesizes that (1) as potential guest molecules become coordinated by water, form nuclei, and begin to grow, nearby inhibitor molecules disrupt the organization of the forming clathrate, and (2) inhibitor molecules bind to the surface of the hydrate crystal precursor and retard further growth along the bound growth plane, resulting in a modified planar morphology. Part one of this mechanism is supported by the results of our molecular dynamics simulations for the four inhibitor molecules studied. PVCap and VIMA, the more effective inhibitors, show strong interactions with the liquid water phase under hydrate-forming conditions, while PVP and PEO appear relatively neutral to the surrounding water.

For part two, we test our hypothesis that the degree of inhibition is related to the strength of the binding of the inhibitor to the surface of the hydrate crystal. We find that the free energy of binding between the inhibitor molecules and the hydrate surface does correlate directly with the effectiveness of the inhibitors. Inhibitors increasing in effectiveness, PEO < PVP < PVCap < VIMA, also have increasingly negative (exothermic) binding energies of $-0.2 < -20.6 < -37.5 < -45.8$ kcal/mol and binding free energies of increasing favorability ($+0.4 \approx +0.5 < -9.4 < -15.1$ kcal/mol). The free energies of binding of PVP and PEO, $+0.5 \pm 3.7$ and $+0.4 \pm 3.9$ kcal/mol respectively, correspond to neutral equilibrium constants, $K_{eq} \cong 1$, for binding reactions, whereas the free energies of binding

for the stronger inhibitors, PVCap and VIMA, result in $K_{eq} \gg 1$. With $K_{eq} \gg 1$ a relatively high fraction of the surfaces of ensuing nuclei would be bound by PVCap and VIMA, disrupting growth. In addition, two molecular characteristics that lead to strongly binding inhibitors were found: (1) a charge distribution on the edge of the inhibitor that mimics the charge separation in the water molecules on the surface of the hydrate and (2) an inhibitor size similar to the available space at the hydrate-surface binding site. These two molecular characteristics result in strong hydrogen bonding between the inhibitor molecule and the surface of a forming hydrate crystal and thus lead to more effective inhibitor molecules.

Acknowledgment. We thank EniTecnologie for their financial support of this research. We also gratefully acknowledge Prof. William Green, Prof. John Deutch, and Dr. Kevin Sparks for their insightful contributions to this work and the other members of our research groups at MIT for their help and support.

JA0554965